ACS Energy LETTERS

http://pubs.acs.org/journal/aelccp

Elucidating Degradation Pathways in Perovskite-Based Water Splitting Devices

Published as part of ACS Energy Letters special issue "The Evolving Landscape of Energy Research: Insights from Leading Researchers".

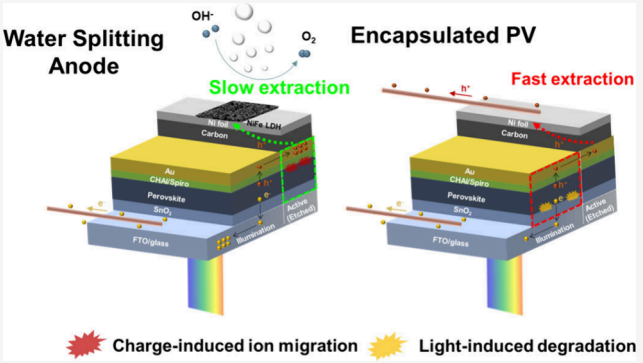
Wooyong Jeong,[†] Chang-Seop Jeong,[†] Juwon Yun,[†] Young Sun Park, Junwoo Lee, Jeongyoub Lee, Chan Uk Lee, Subin Moon, Soobin Lee, Sumin Kim, Jun Hwan Kim, Sang Yeop Park, Donghyun Kim, Seonyoo Kim, Jaeeon Lim, Jeongjun Lee, Hyein An, and Jooho Moon*

Cite This: *ACS Energy Lett.* 2025, 10, 4758−4768

Read Online

ACCESS | Metrics & More | Article Recommendations | Supporting Information

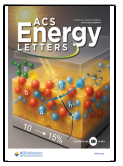
ABSTRACT: **Despite recent encapsulation strategies that suppress moisture-induced degradation and support high-performance operation, perovskite-based water splitting devices still exhibit limited operational stability. This instability originates from the slower consumption of photocarriers, compared with photovoltaic (PV) cells, which exacerbates charge accumulation at the catalyst/electrolyte interface. Herein, *in situ* and *ex situ* studies track how this intense charge buildup governs a distinct degradation pathway in water splitting anodes relative to encapsulated perovskite PV cells. Our observations show that the anodes undergo a charge-induced failure process: accelerated iodine migration triggers defect formation at the hole transport layer/perovskite interface located directly beneath the electrochemically active region. In contrast, encapsulated PV cells experience light-induced degradation within the illuminated area, where defects emerge only after extended operation and at the electron transport layer/perovskite interface. These results clarify that perovskite-based water splitting devices follow a distinct, electrochemically driven degradation mechanism, providing insights for designing more stable perovskite-based electrochemical systems.**



After the successful demonstration of high-performance perovskite solar cells (PSCs), extensive efforts have been directed toward integrating perovskite materials into water splitting devices.[1−3] Considering the inherent moisture sensitivity of perovskites, initial research focused on developing encapsulation strategies that prevent direct contact between the electrolyte and the perovskite layer. Protective barriers such as epoxy, fusible metals, metal foils, and carbon layers have therefore been widely applied to perovskite-based electrochemical devices operated in aqueous media.[4−8] Once water ingress was effectively blocked, research efforts to enhance performance and stability shifted toward interface and catalyst engineering. These studies confirmed the crucial role of interface design in water splitting performance and underscored the importance of catalysts in enhancing both efficiency and durability.[4,9,10] Despite these advancements, the operational stability of immersed perovskite-based water splitting devices remains significantly lower than that of PSCs, indicating the presence of degradation mechanisms unique to water splitting operation.

The principal difference between PSCs and immersed perovskite-based water splitting systems is the time scale on which photocarriers are consumed. In PSCs, photogenerated carriers are extracted through an external circuit within nanoseconds to microseconds, enabling rapid charge collection and minimal buildup.[11] However, in water splitting devices, the transport of photogenerated carriers to the catalyst surface occurs on the nanosecond to microsecond time scale, whereas their consumption through electrochemical reactions requires milliseconds to seconds. This disparity means that carriers are supplied much faster than they are consumed, resulting in charge accumulation at the catalyst/electrolyte interface.[12−14]

Received: June 30, 2025
Revised: August 29, 2025
Accepted: September 3, 2025
Published: September 5, 2025



Downloaded via YONSEI UNIV on December 10, 2025 at 00:55:51 (UTC).
See https://pubs.acs.org/sharingguidelines for options on how to legitimately share published articles.

ACS Publications

© 2025 American Chemical Society

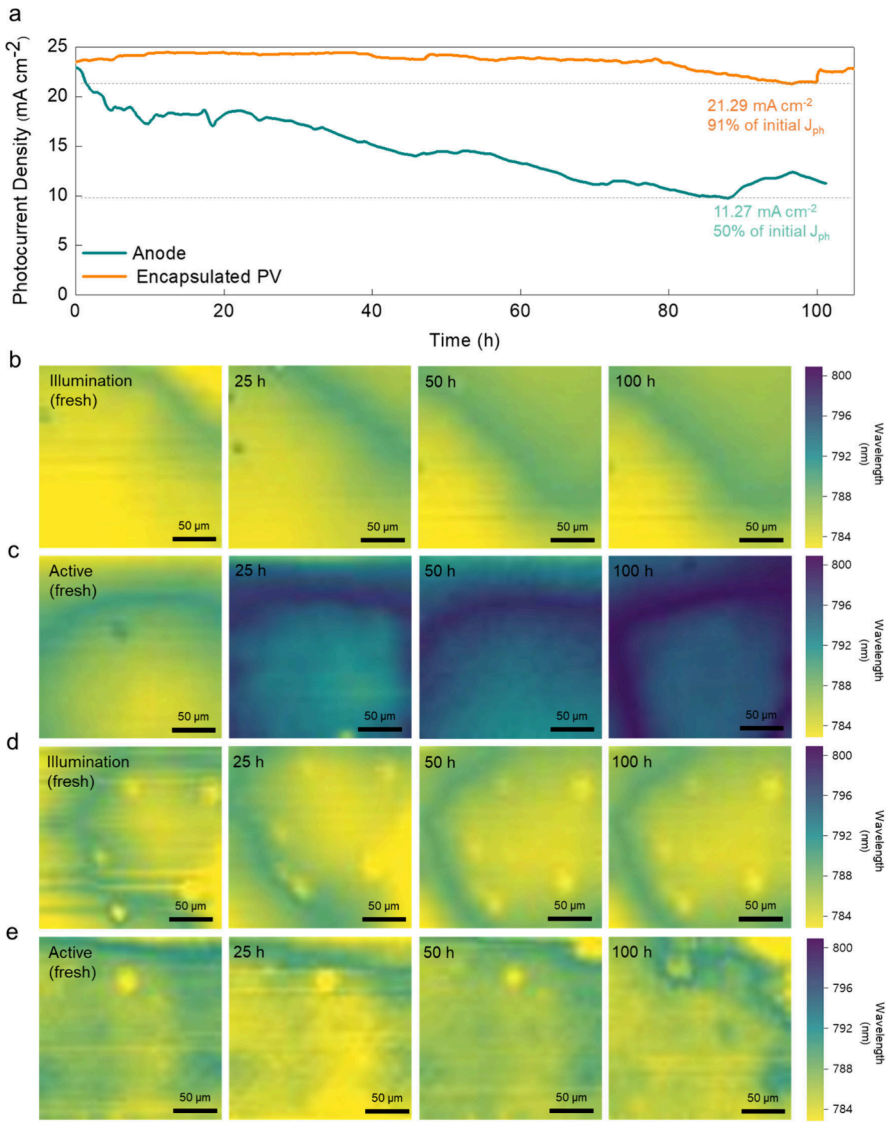


Figure 1. (a) Long-term operational stability of the perovskite water splitting anode and the encapsulated PV device, recorded at 1.23 V_{RHE} and 0 V, respectively, under continuous 1-sun illumination in 1 M KOH (pH 14). *In situ* PL mapping images collected during the stability test for (b) the illuminated area of the water splitting anode, (c) active area of water splitting anode, (d) illuminated area of the encapsulated PV device, and (e) the active area of the encapsulated PV device.

Unlike the conventional charge buildup that develops at the perovskite/transport layer interface, accumulation at the catalyst/electrolyte boundary differs greatly in magnitude and spatial distribution. Consequently, the degradation pathways in perovskite water splitting cells differ fundamentally from those in PSCs. PSCs primarily degrade through interfacial recombination or material decomposition under illumination; however, the intense charge buildup in water splitting cells can trigger additional failure processes driven by prolonged exposure to stored charges.[4,9,15,16] Understanding these unique pathways is therefore essential for devising strategies that extend the stability and service life of perovskite water splitting devices.

To investigate these mechanisms, we examined two devices that share an identical n−i−p perovskite and transport layers configuration: one operated as the anode in a water splitting setup (denoted "water splitting anode"; see Supporting Note S1) and the other as an encapsulated photovoltaic cell ("encapsulated PV"; Figure S1). Through combined *in situ* and *ex situ* analyses, we show that charge accumulation at the catalyst/electrolyte interface expedites iodine migration toward the hole-transport-layer (HTL)/perovskite interface within the active region beneath the catalytic area. In contrast, degradation in the encapsulated PV devices is dominated by light-induced processes that generate defects at the perovskite/electron transport layer (ETL) interface inside the illuminated region, where iodide migrates into trap states at that boundary. These findings directly link charge accumulation to accelerated perovskite degradation during water splitting operation and demonstrate a failure mechanism distinct from that observed under conventional PV operation.

The device structure and performance of the PSCs are summarized in Supporting Note S2. Based on the PSC device architecture, we fabricated a perovskite-based water splitting anode by first spreading carbon powder on top of the Au layer, followed by attaching a Ni foil layered with NiFe-layered double hydroxide (LDH)@Ni foam catalyst. For the encapsulated PV device, carbon powder and Ni foil were applied in the same manner, after which a Cu wire was placed

https://doi.org/10.1021/acsenergylett.5c02009
ACS Energy Lett. 2025, 10, 4758−4768

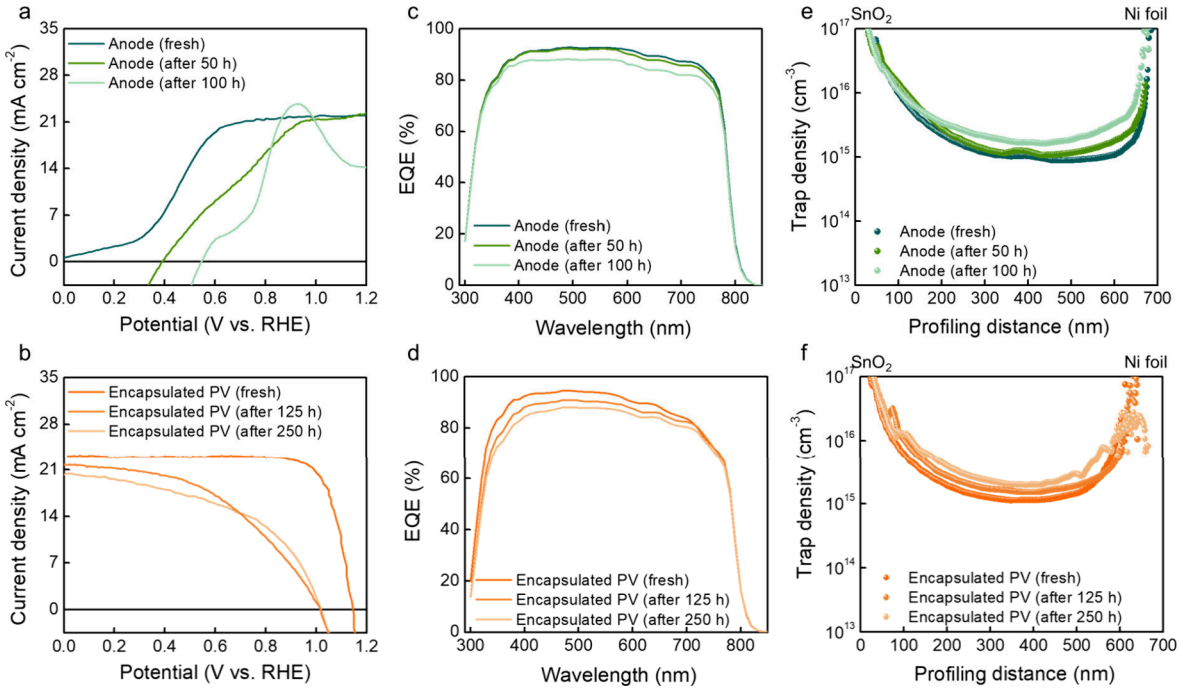


Figure 2. LSV curves of (a) perovskite water splitting anodes measured at 0 h (fresh) and after 50 and 100 h of operation, and (b) encapsulated PV devices measured at 0 h (fresh) and after 125 and 250 h of operation. EQE spectra of (c) anodes and (d) encapsulated PV devices at the indicated time points. Spatial distributions of trap densities for (e) anodes and (f) encapsulated PV devices.

on top of the Ni foil. Substituting the catalyst with a Cu wire allowed the encapsulated PV device to preserve the operating conditions of a standard PSC while mirroring the anode's physical stack (see Figure S1 and the Experimental section for details). Device performance was evaluated by linear sweep voltammetry (LSV) under 1-sun illumination in 1 M KOH (pH 14) (Figure S2). The immersed anode delivered a photocurrent density (J_{ph}) of 21.58 mA cm^{-2} at 1.23 V_{RHE} (V *vs.* reversible hydrogen electrode), an onset voltage (V_{on}) of 0.18 V_{RHE}, and a fill factor (FF) of 57.33%. In contrast, the encapsulated PV device yielded a J_{ph} of 22.16 mA cm^{-2} at 0 V, a V_{on} of 1.15 V, and an FF of 79.13%. The lower fill factor and photocurrent densities of the water splitting anode are attributed to additional electrochemical resistance and slower reaction kinetics. Results for 12 separate devices are summarized in Figure S3−S5, demonstrating consistent performance results of both configurations.

The operational stability of the water splitting anode and the encapsulated PV device was evaluated using chronoamperometry under continuous 1-sun illumination in 1 M KOH (pH 14) electrolyte (at 1.23 V_{RHE} for the water splitting anode and 0 V for the encapsulated PV device) (Figure 1a). The J_{ph} of the water splitting anode declined rapidly, dropping to below 50% of its initial value within 100 h of operation. In contrast, the encapsulated PV device exhibited high operational stability over the same period, maintaining 91% of its initial J_{ph}. The operational stability statistics for both devices are presented in Figure S6, highlighting the superior operational stability of the encapsulated PV device. The significant difference in operational stability is attributed to charge accumulation in the water splitting anode, stemming from the slow kinetics of the EC reaction. Note that no degradation was observed for anode samples immersed in electrolyte for 100 h without operation, indicating that the encapsulation effectively prevented any contact between electrolyte and perovskite (Figure S7). Digital photographs of the tested devices further show that the black phase of the perovskite remained intact, which strongly suggests that the failure originates from internal degradation processes occurring during operation rather than from electrolyte intrusion (Figure S8). To investigate the impact of this charge accumulation on perovskite degradation, *in situ* photoluminescence (PL) mapping was conducted during the stability test (Figure 1b−e). Two distinct regions were analyzed: the illuminated area, which is directly exposed to light, and the active area, located directly beneath the Ni foil (see Figure S1). This region-specific analysis aimed to (1) determine whether charge accumulation has a greater effect on the perovskite region directly beneath the catalyst/electrolyte interface and (2) assess whether lateral degradation occurs. Note the grains observed in PL images are likely to be residue or marks formed on the glass side of the device due to electrolyte evaporation and the electrolyte level was maintained by continuously supplying fresh electrolyte. For the water splitting anode, the active area showed a PL peak shift toward longer wavelengths after 25 h of operation, attributed to iodine migration that induces phase segregation into an iodide-rich phase.[17,18] Despite this degradation in the active area, the PL peak in the illumination area remained unchanged, retaining its original spectral characteristics. Even with extended operation, the PL shift was confined to the active area, while the illumination area appeared largely unaffected. Furthermore, analysis at the boundary between the active and illuminated areas revealed that phase segregation originating in the active region gradually extended into the illuminated region over time (Figure S9). These findings indicate that charge accumulation at the catalyst/electrolyte interface initially impacts the active area and then propagates degradation laterally toward the illuminated region. In contrast, the encapsulated PV device exhibited no PL shift in either region after 100 h of operation, confirming its stable

https://doi.org/10.1021/acsenergylett.5c02009
ACS Energy Lett. 2025, 10, 4758−4768

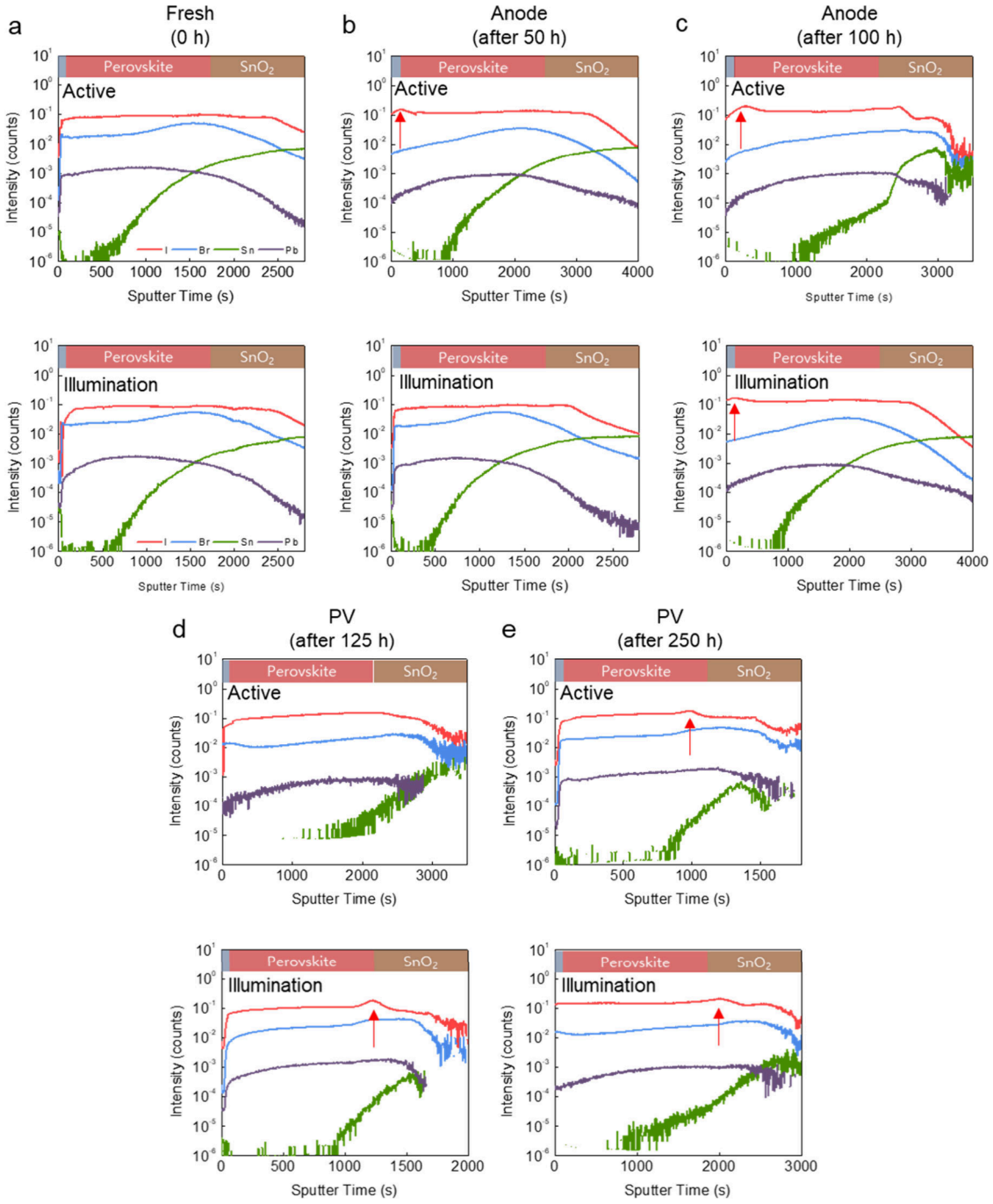


Figure 3. ToF-SIMS depth profiles for perovskite-based water splitting anodes and encapsulated PV devices at each operating condition: (a) 0 h (fresh), (b) anode after 50 h, (c) anode after 100 h, (d) encapsulated PV (after 125 h), and (e) encapsulated PV (after 250 h).

performance relative to the water splitting anode. After an extended operation of 300 h, degradation appeared, originating from the illuminated area (Figure S10). This behavior is attributed to the absence of charge accumulation beneath the Ni foil, due to the immediate extraction of photogenerated holes via the Cu wire, unlike in the water splitting anode. Consequently, degradation in the encapsulated PV device is more strongly influenced by light exposure, which contrasts with the charge-accumulation-driven degradation observed in the water splitting anode. These results demonstrate that charge accumulation caused by the slow kinetics of the EC reaction significantly accelerates perovskite degradation and induces a degradation pathway distinct from that observed in conventional PV operation.

To further investigate the changes in bulk characteristics during operation, we fabricated a hybrid device that combines the architectures of a perovskite water splitting anode and an encapsulated PV cell (Figure S11 and Supporting Note S3). This configuration allows simultaneous tracking of perovskite carrier dynamics during anode operation in a two-electrode setup and concurrent evaluation of both anode and PV modes within the same specimen.[19] Figure 2a, b present LSV for the water splitting mode obtained under 1-sun illumination in 1 M KOH at the initial state (0 h) and after two sequential stability intervals tests (50 and 100 h). Similarly, the PV mode was

https://doi.org/10.1021/acsenergylett.5c02009
ACS Energy Lett. 2025, 10, 4758−4768

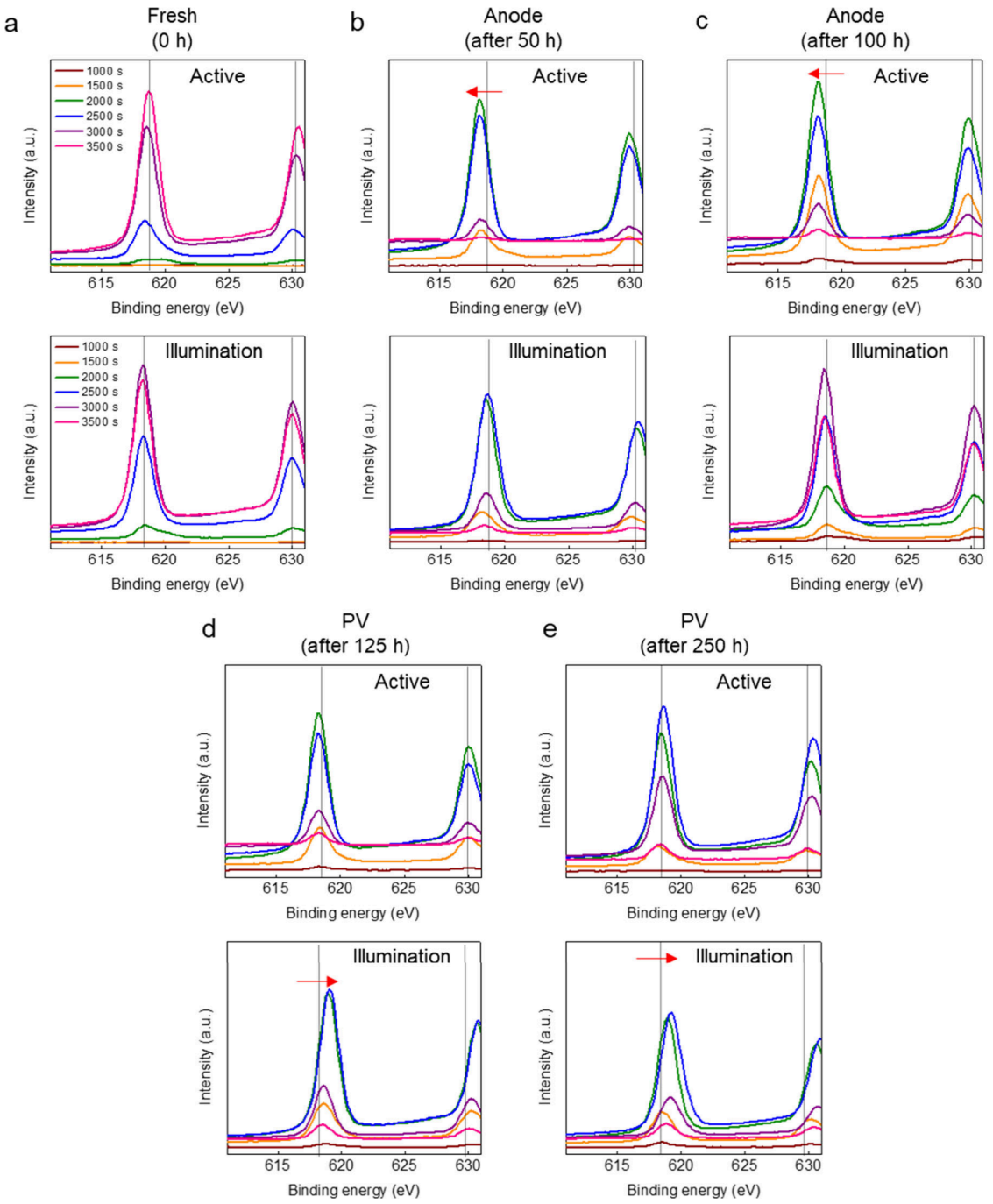


Figure 4. XPS depth spectra of the I $3d_5$ peaks of perovskite-based water splitting anode and encapsulated PV devices at different etching durations (1000, 1500, 2000, 2500, 3000, and 3500 s): (a) 0 h (fresh), (b) anode (after 50 h), (c) anode (after 100 h), (d) encapsulated PV (after 125 h), and (e) encapsulated PV (after 250 h).

characterized at 0 h and following two consecutive stability tests (125 and 250 h). Corresponding long-term stability traces are provided in Figure S12. After the first stability interval, both modes exhibited reductions in V_{on} and FF, while the photocurrent density, measured at 1.23 V_{RHE} for the anode and 0 V for the PV device, remained unchanged. As operation time progressed, the anode mode experienced pronounced degradation across all metrics, retaining only ∼60% of its initial photocurrent. The PV mode likewise showed significant declines in V_{on} and FF yet preserved ∼70% of its initial photocurrent. Mott−Schottky analysis revealed a decrease in built-in voltage (V_{Bi}) with increasing operation time for both modes, mirroring the reductions in V_{on} and FF observed in the LSV data (Figure S13).

To verify the performance degradation associated with efficiency losses in specific wavelength regions, we performed external quantum-efficiency (EQE) measurements on both operation modes (Figure 2c, d). In agreement with the LSV trends in Figure 2a, b, the integrated EQE of the anode and PV configurations declined progressively with increasing operation time. However, the spectral domains most affected differed distinctly. The PV mode displayed its largest decrease in the short-wavelength range (λ < 500 nm), whereas the anode mode showed the most pronounced degradation at longer

https://doi.org/10.1021/acsenergylett.5c02009
ACS Energy Lett. 2025, 10, 4758−4768

wavelengths (600−800 nm). Because lower-energy photons penetrate more deeply into the absorber, the long-wavelength EQE loss observed for the anode indicates that degradation initiates at the upper interface, the spiro-OMeTAD/perovskite junction.[20,21] In contrast, the PV mode's short-wavelength loss implies degradation in the perovskite bulk or at the lower interface (perovskite/ETL(SnO_2)). To connect these optical findings to defect formation, we employed drive-level capacitance profiling (DLCP) and capacitance−voltage (*C*−*V*) analysis on both modes at 0 h (fresh) and after two sequential stability tests (Figure S14).[22,23] Depth-resolved trap-density profiles extracted from these measurements (Figure 2e, f) reveal a gradual increase in trap density with operating time for both configurations, yet the spatial origin of the traps diverges. Consistent with the EQE results, the PV mode exhibits its largest trap-density increase in the perovskite bulk and near the perovskite/SnO_2 interface. In contrast, the anode mode shows a substantially greater rise in trap density at the spiro-OMeTAD/perovskite interface than at the ETL side, and this imbalance intensifies with longer operation. The *in situ* PL maps in Figure 1 corroborate these observations. Under PV operation, degradation begins in the illuminated region because prolonged photon exposure drives perovskite decomposition. Under anode operation, however, degradation originates at the top of the active area, where sluggish electrochemical kinetics cause sustained hole accumulation. We attribute the pronounced trap formation at the spiro-OMeTAD/perovskite junction to accelerated iodide migration promoted by this hole build-up. Iodide-related defects possess lower activation energies for migration than other ionic species and therefore drift readily toward regions of high hole density.[24] Their accumulation induces phase segregation within the perovskite lattice, a pathway widely recognized as a primary degradation pathway in perovskite-based optoelectronic devices.[25−27]

Next, time-of-flight secondary-ion mass spectrometry (ToF-SIMS) was performed from the top surface to the bottom contact to track ion migration behavior (Figure 3a−e). All *ex situ* measurements required removal of the epoxy encapsulant at specified intervals; this procedure peeled away the Au electrode, leaving the HTL as the uppermost layer (Figure S15). In the fresh sample (0 h), the ion distributions in both the active and illumination regions were nearly identical, confirming compositional uniformity across the device (Figure 3a). However, after 50 h of operation in the water splitting anode, a pronounced accumulation of I ions appeared at the upper HTL/perovskite interface in the active region, whereas no significant change was detected in the illumination region (Figure 3b). This observation agrees with earlier results showing that degradation initiates at the top of the active area during anode operation. After 100 h, an elevated concentration of I ions was also detected at the upper interface of the illuminated region, mirroring the distribution in the active region (Figure 3c). These data indicate that degradation, once triggered in the active region, propagates laterally and eventually affects the illuminated portion of the device. In contrast, a different evolution was observed under PV operating conditions. After 125 h, the active region showed no detectable change, yet an increased I ions emerged at the lower perovskite/SnO_2 interface in the illumination region (Figure 3d), consistent with ion migration toward trap states at that boundary. After 250 h of operation, both regions exhibited heightened I ion concentrations at their bottom interfaces (Figure 3e). Thus, whereas degradation in the water splitting anode originates at the upper HTL/perovskite interface of the active region, degradation in the PV configuration begins in the perovskite bulk or at the ETL interface of the illuminated region.

To gain deeper insight into the ion migration observed in the ToF-SIMS analysis, X-ray photoelectron spectroscopy (XPS) depth analysis was also performed from the top surface to the bottom of the devices. The variation of the I/Pb atomic ratio in fresh samples obtained from both ToF-SIMS and XPS as a function of sputtering time is organized in Supporting Note S4. Elemental depth profiles of the anode samples show that the atomic concentrations of I and Pb progressively increase toward the upper HTL/perovskite interface in the active area with increasing operation time (Figure S16). Notably, after 100 h of operation, a similar enrichment of I and Pb near the HTL interface was observed in the illumination area as well, providing direct evidence of lateral degradation, which is consistent with the previous *in situ* PL and DLCP results. In PV devices, a gradual increase in the I and Pb signals toward the bottom perovskite/ETL interface with prolonged operation further supports the trends observed in the ToF-SIMS depth profiles. To investigate the chemical states of iodine in more detail, XPS depth spectra were acquired at various etching durations (1000−3500 s), focusing on regions exhibiting high iodine concentrations (Figure 4a−e; complete spectra provided in Figure S17). In the water splitting anode samples, the I $3d_5$ peak in the active area shifted progressively toward lower binding energies with increasing operation time, indicating the accumulation of migrated I ions and the formation of iodide-rich phases resulting from upward ion migration (Figure 4b, c). In contrast, the PV devices exhibited a shift in the I $3d_5$ peak toward higher binding energies near the ETL interface in the illumination area over time (Figure 4d, e). This spectral evolution suggests light-induced degradation due to migrated I ions near the perovskite/ETL interface, including the formation of PbI_2 and its subsequent oxidative conversion into metallic Pb^0 and molecular iodine (I_2) or neutral iodine species (I^0).[28,29] These observations are further corroborated by the XPS depth spectra of Pb (Figure S18). In the water splitting anode after 100 h of operation, the Pb 4f signal near the upper interface remained largely unchanged, while the Pb signal in the bulk region exhibited a pronounced shift toward higher binding energies. This shift likely reflects a localized decrease in electron density caused by the migration of I ions toward the HTL interface. Conversely, in PV devices after 250 h of operation, the Pb 4f peak near the ETL interface shifted toward lower binding energies. This result aligns with the presence of light-induced degradation products, such as PbI_2 and metallic Pb^0, corroborating the I $3d_5$ peak trends and supporting the proposed degradation mechanism.

Kelvin probe force microscopy (KPFM) was employed to complement the *in situ* optoelectronic and *ex situ* chemical analyses. This enables local work-function variations across defined regions, thereby revealing changes in electronic band structure and charge transport efficiency that develop during operation.[30] The fresh sample (0 h) exhibited an average HTL work function of 4.51 eV (Figure S19), consistent with reported values for spiro-OMeTAD.[31] After 50 h of operation, the HTL work function in the water splitting anode increased by 0.28 eV in the active region and by 0.15 eV in the illuminated region (Figure 5a: solid and dashed lines in dark

https://doi.org/10.1021/acsenergylett.5c02009
ACS Energy Lett. 2025, 10, 4758−4768

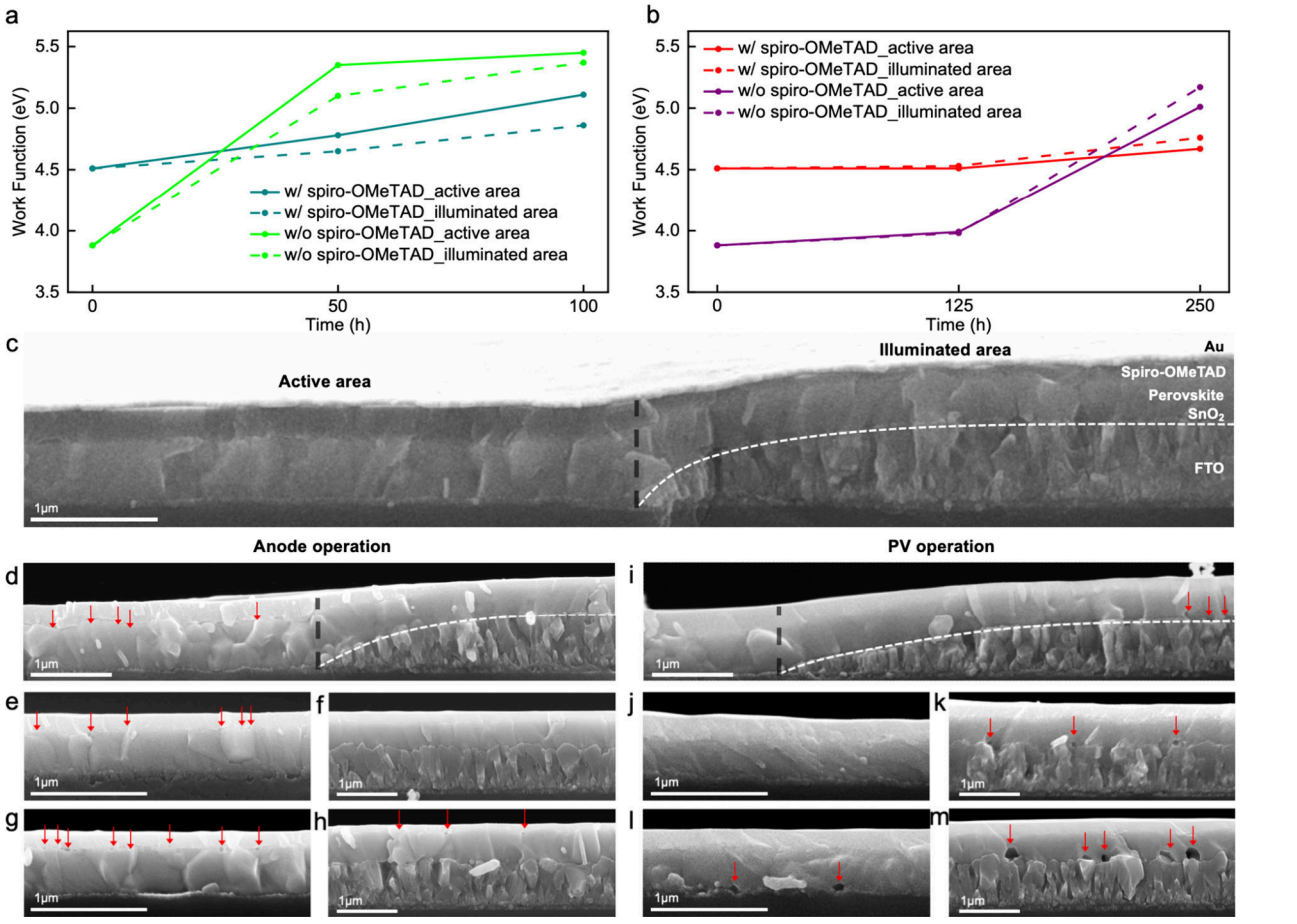


Figure 5. Time-dependent work function values obtained by KPFM for (a) water splitting anodes and (b) encapsulated PV cells. Low-magnification cross-sectional SEM images of (c) the fresh device (0 h), (d) the anode-operated device after 50 h, and (i) the PV-operated device after 125 h. High-magnification images of the anode's active region after (e) 50 h and (g) 100 h and of the illuminated region after (f) 50 h and (h) 100 h. High-magnification images for PV operation at the active region after (j) 125 h and (l) 250 h, and at the illuminated region after (k) 125 h and (m) 250 h.

cyan, and Figure S20). Continued operation to 100 h intensified the shift, reaching 4.86 eV in the illuminated region and 5.11 eV in the active region. The spatial and temporal evolution of these shifts indicates that charge accumulation originates beneath the active region and subsequently propagates laterally toward the illuminated region. This accumulation drives iodide migration toward the HTL, as corroborated by the ToF-SIMS and XPS data. The migrated iodide is further oxidized to I_2 or I_3^- by the local hole accumulation, chemically oxidizing spiro-OMeTAD and thereby raising its work function.[32−34] These findings align well with observations made through *in situ* characterization methods. To assess the perovskite layer directly, each water splitting anode was rinsed with chlorobenzene (CB) to remove the organic HTL, exposing the perovskite surface. Note that the KPFM measurements for the CB-washed samples were performed after storing them in a vacuum chamber for 6 h following the washing process, showing no signs of artifacts (Figure S21−S23). The fresh perovskite displayed a work function of 3.88 eV (Figure S19). After 50 h, the active region's value rose to 5.35 eV and further to 5.45 eV after 100 h (Figure 5a: solid and dashed lines in bright green, and Figure S24). The earlier and larger shift in the active region again underscores localized degradation. The abrupt increase, exceeding 1.5 eV, implies formation of an iodide-rich phase.[29,35] Furthermore, the pronounced accumulation of positive charge in the HTL raises the work function at both the HTL surface and the HTL/perovskite interface. This shift induces downward band bending at these junctions, accounting for the marked decline in V_{on} after extended operation. Atomic force microscopy (AFM) measurements of CB-washed anodes reveal a substantial increase in surface roughness beneath the active region, implying pinhole formation caused by severe defect generation at the HTL/perovskite interface (Figure S25). In contrast, in the encapsulated PV devices, the work function in both regions showed negligible change after operation, remaining close to its initial value of 4.51 eV (Figure 5b: solid and dashed lines in red, and Figure S26). Similarly, after HTL removal via CB washing, the surface potential exhibited minimal variation after 125 h, with only ∼0.1 eV change detected in both regions (Figure 5b: solid and dashed lines in purple, and Figure S27). After 250 h, a more noticeable increase in the work function was observed in the illuminated area. This rise is likely attributed to light-induced degradation caused by prolonged light exposure. In contrast to the water splitting anode, the average surface roughness of the perovskite layer in PV devices did not show significant change over 250 h of operation (Figure S28), indicating a distinct degradation pathway. To further characterize the topographical changes observed via AFM, cross-sectional scanning electron micros-

https://doi.org/10.1021/acsenergylett.5c02009
ACS Energy Lett. 2025, 10, 4758−4768

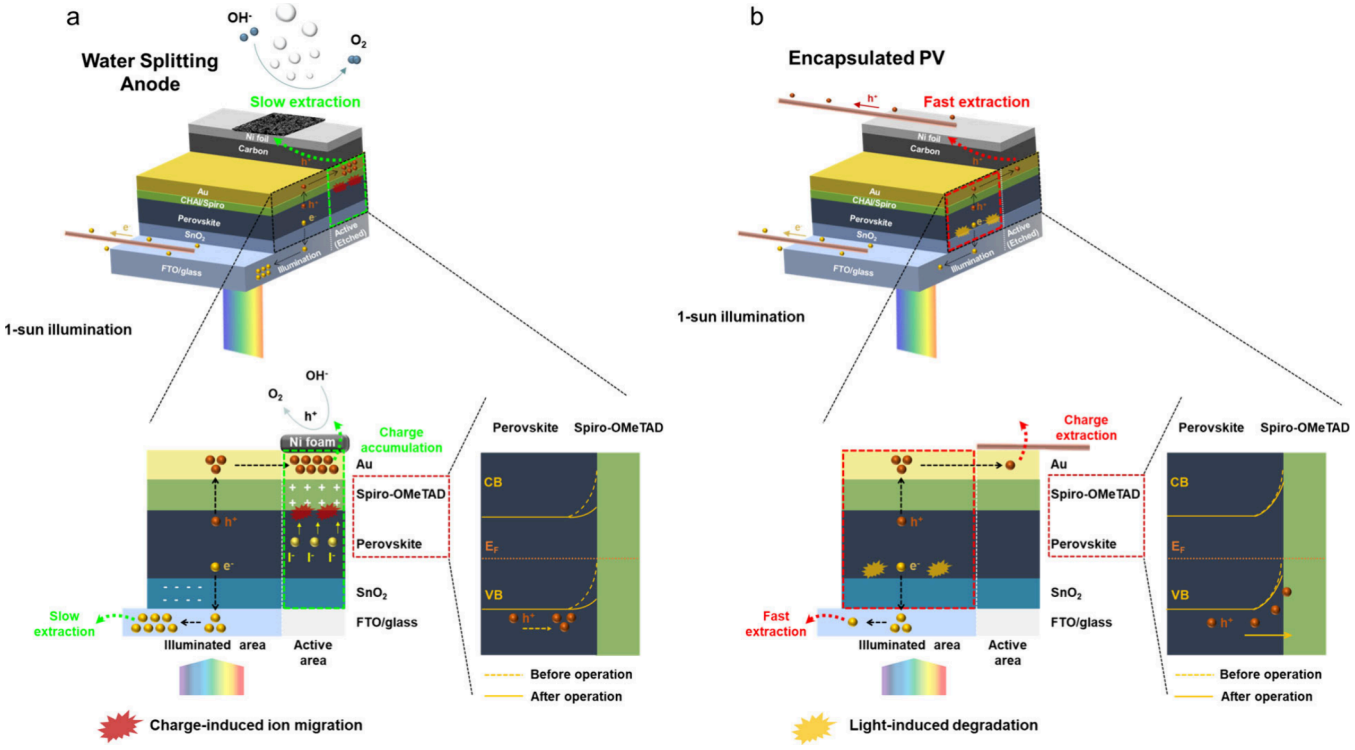


Figure 6. Schematic illustration of the degradation mechanisms in (a) a perovskite-based water splitting anode and (b) an encapsulated PV device.

copy (SEM) was conducted. Figure 5c delineates the illumination and active areas, distinguished by the presence of the bottom FTO contact. In water splitting anode samples, pinholes at the HTL/perovskite interface beneath the active area emerged after 50 h of operation, while no pinholes were observed in the illuminated area (Figure 5d–f). After 100 h, significant pinhole formation was identified in the active area, along with a few pinholes appearing in the illumination area (Figure 5g, h). These results suggest that the increased surface roughness detected by AFM in the active area corresponds to pinhole formation driven by charge accumulation at the catalyst/electrolyte interface. These pinholes likely serve as nucleation sites for further defect formation, ultimately accelerating device degradation.[36] In contrast, PV devices exhibited pinholes at the perovskite/ETL interface within the illumination area after 125 h of operation (Figure 5i–k). These defects became more prominent after 250 h and were also observed in the active area. This behavior correlates well with EQE and DLCP measurements, indicating that degradation in PV devices originates at the perovskite/ETL interface. The combined use of KPFM and SEM allowed for direct observation of both surface potential changes and pinhole formation, enabling identification of different initial degradation sites and validating the interface-driven degradation mechanisms revealed through *in situ* characterizations.

Figure 6 schematically summarizes the degradation mechanisms in the perovskite-based water splitting anode and the encapsulated PV device. In the water splitting anode, the temporal mismatch between carrier supply and consumption results in pronounced charge accumulation at the catalyst/electrolyte interface, which particularly influences the boundary potential at the upper layer of the active area. This boundary potential subsequently intensifies the local electric field across the perovskite layer, thereby accelerating iodide migration toward the perovskite/HTL interface and resulting in spiro-OMeTAD oxidation as well as phase segregation into iodide-rich domains within the perovskite. Experimentally, the degradation is evidenced by a red-shifted PL spectrum, elevated iodide concentration, and increased trap density at the HTL/perovskite interface. Pinhole formation subsequently develops and spreads laterally from the active to the illuminated region, ultimately compromising both structural integrity and performance. Moreover, owing to the significantly increased iodine concentration near the HTL/perovskite interface of active area, lateral diffusion migration becomes active, resulting in substantial accumulation of iodine ions even in the upper regions of the illuminated area within 100 h of operation (see Supporting Note S5 for detailed explanation of lateral ion migration). In contrast, in the encapsulated PV device, rapid charge extraction through the external circuit prevents charge accumulation in the active area. Degradation primarily occurs at the perovskite/ETL interface within the illumination area, initiated by the migration of iodine ions to interfacial trap states at the perovskite/metal oxide interface (i.e., light-induced phase segregation). With prolonged light exposure, perovskite decomposition occurs both in the bulk and at the perovskite/ETL interface, leading to the formation of PbI_2 and I_2 phases. This degradation results in efficiency losses predominantly in the short-wavelength region (λ < 500 nm), indicating that the degradation originates from the bulk perovskite and the perovskite/ETL interface. The formation of significant pinholes at the perovskite/ETL interface in the illumination area, along with the lateral propagation of degradation toward the active area, highlights a degradation pathway that is primarily governed by the duration of light exposure. In encapsulated PV devices, intrinsic defects in the perovskite crystal structure, such as vacancies or interstitial ions, are activated under illumination, facilitating the migration

https://doi.org/10.1021/acsenergylett.5c02009
ACS Energy Lett. 2025, 10, 4758–4768

of ionic species, particularly halide or metal ions. This process is believed to proceed gradually through localized chemical imbalances, leading to photodegradation, as the absence of charge accumulation limits the acceleration of decomposition. In contrast, charge accumulation can rapidly accelerate degradation, primarily due to the formation of a strong electric field at the interface, which promotes iodine ion migration despite the inherently slow kinetics of electrochemical reactions. Therefore, it can be inferred that encapsulated PV devices undergo a relatively slower degradation process. In addition, the thickness of the hole-accumulation layer was estimated from the variation in depletion region width (Supporting Note S6). These findings underscore the key distinction in degradation mechanisms: while PV device degradation is predominantly light-driven, water splitting anodes degrade due to charge accumulation at the catalyst/electrolyte interface. We additionally analyzed the stability degradation trend with a solar cell externally wired to an electrocatalyst to further support the degradation mechanism (Supporting Note S7). Schematic demonstrating of every *in/ex situ* characterization is illustrated in the Figure S29−33)

Based on these insights, we propose two major strategies to enhance the stability of perovskite-based water splitting anodes: (1) employing a chemically robust absorber layer and (2) improving electrochemical reaction kinetics. Compared to conventional OIHPs, all-inorganic perovskites such as $CsPbI_3$ offer superior structural and chemical stability under operational stress, making them more suitable for long-term use. Simultaneously, improving the kinetics of the water splitting reactions is essential to mitigate charge accumulation. This can be achieved by developing high-performance catalysts or incorporating materials that enable faster interfacial reaction rates. These strategies accelerate sluggish electrochemical processes, thereby enhancing both performance and durability. Ultimately, integrating robust absorber materials with kinetic enhancement approaches could significantly improve the operational stability of perovskite-based water splitting anodes, bringing them closer to the performance levels of commercial PV devices and accelerating progress toward practical solar fuel technologies.

In summary, we conducted a systematic investigation of degradation pathways in perovskite-based solar water splitting devices that are fully protected against moisture-induced decay and compared them directly with encapsulated perovskite PV counterparts. A combination of *in situ* and *ex situ* analyses allowed us to pinpoint both the location and the nature of degradation in each configuration. For the water splitting anode, degradation originates at the HTL/perovskite interface in the active region, where prolonged charge accumulation at the catalyst/electrolyte interface drives iodide migration toward the HTL, an unequivocal signature of charge-induced degradation. In contrast, in the PV device, degradation is more pronounced at the perovskite/ETL interface within the illuminated region; here, iodide migrates toward the ETL under continuous illumination, forming PbI_2 and reflecting a light-induced degradation pathway. These results demonstrate that perovskite-based water splitting systems follow degradation routes that differ fundamentally from those in conventional perovskite PV cells. The observed spatial and temporal variations in ion migration highlight the critical role of charge accumulation at electrochemical interfaces. Addressing this accumulation through targeted interface and catalyst engineering is therefore essential for improving the long-term operational stability of perovskite-based water splitting devices.

■ ASSOCIATED CONTENT

Supporting Information

The Supporting Information is available free of charge at https://pubs.acs.org/doi/10.1021/acsenergylett.5c02009.

Experimental procedure. AFM surface topography and XRD patterns of perovskite. J-V curves of PSC. LSV curves and operational stability of perovskite-based anode and encapsulated PV devices. XPS and capacitance analysis of perovskite-based anode and encapsulated PV devices (PDF)

■ AUTHOR INFORMATION

Corresponding Author

Jooho Moon − *Department of Materials Science and Engineering, Yonsei University, Seoul 03722, Republic of Korea;* orcid.org/0000-0002-6685-9999; Email: jmoon@yonsei.ac.kr

Authors

Wooyong Jeong − *Department of Materials Science and Engineering, Yonsei University, Seoul 03722, Republic of Korea*

Chang-Seop Jeong − *Department of Materials Science and Engineering, Yonsei University, Seoul 03722, Republic of Korea*

Juwon Yun − *Department of Materials Science and Engineering, Yonsei University, Seoul 03722, Republic of Korea*

Young Sun Park − *Department of Materials Science and Engineering, Yonsei University, Seoul 03722, Republic of Korea*

Junwoo Lee − *Department of Materials Science and Engineering, Yonsei University, Seoul 03722, Republic of Korea*

Jeongyoub Lee − *Department of Materials Science and Engineering, Yonsei University, Seoul 03722, Republic of Korea*

Chan Uk Lee − *Department of Materials Science and Engineering, Yonsei University, Seoul 03722, Republic of Korea*

Subin Moon − *Department of Materials Science and Engineering, Yonsei University, Seoul 03722, Republic of Korea*

Soobin Lee − *Department of Materials Science and Engineering, Yonsei University, Seoul 03722, Republic of Korea*

Sumin Kim − *Department of Materials Science and Engineering, Yonsei University, Seoul 03722, Republic of Korea*

Jun Hwan Kim − *Department of Materials Science and Engineering, Yonsei University, Seoul 03722, Republic of Korea*

Sang Yeop Park − *Department of Materials Science and Engineering, Yonsei University, Seoul 03722, Republic of Korea*

Donghyun Kim − *Department of Materials Science and Engineering, Yonsei University, Seoul 03722, Republic of Korea*

https://doi.org/10.1021/acsenergylett.5c02009
ACS Energy Lett. 2025, 10, 4758−4768

Seonyoo Kim − *Department of Materials Science and Engineering, Yonsei University, Seoul 03722, Republic of Korea*
Jaeeon Lim − *Department of Materials Science and Engineering, Yonsei University, Seoul 03722, Republic of Korea*
Jeongjun Lee − *Department of Materials Science and Engineering, Yonsei University, Seoul 03722, Republic of Korea*
Hyein An − *Department of Materials Science and Engineering, Yonsei University, Seoul 03722, Republic of Korea*

Complete contact information is available at: https://pubs.acs.org/10.1021/acsenergylett.5c02009

Author Contributions

†W.J., C.-S.J., and J.Y. contributed equally.

Notes

The authors declare no competing financial interest.

■ ACKNOWLEDGMENTS

This research was supported by the National R&D Program through the National Research Foundation (NRF) of Korea (No. 2021R1A3B1068920 and 2021M3H4A1A03049662) funded by the Ministry of Science and ICT. This research was also supported by the Yonsei Signature Research Cluster Program of 2021 (2021-22-0002) and the Yonsei Fellowship, funded by Lee Youn Jae.

■ REFERENCES

(1) Fehr, A. M. K.; Agrawal, A.; Mandani, F.; Conrad, C. L.; Jiang, Q.; Park, S. Y.; Alley, O.; Li, B.; Sidhik, S.; Metcalf, I.; et al. Integrated halide perovskite photoelectrochemical cells with solar-driven water-splitting efficiency of 20.8. *Nat. Commun.* **2023**, *14*, 3797.
(2) Jeong, W.; Jang, G.; Yun, J.; Jeong, C.-S.; Park, Y. S.; Lee, H.; Son, J.; Lee, C. U.; Lee, J.; Lee, J.; et al. Large-area all-perovskite-based coplanar photoelectrodes for scaled-up solar hydrogen production. *Energy Environ. Sci.* **2024**, *17*, 3604−3617.
(3) Hansora, D.; Yoo, J. W.; Mehrotra, R.; Byun, W. J.; Lim, D.; Kim, Y. K.; Noh, E.; Lim, H.; Jang, J. W.; Seok, S. I.; et al. All-perovskite-based unassisted photoelectrochemical water splitting system for efficient, stable and scalable solar hydrogen production. *Nat. Energy* **2024**, *9*, 272−284.
(4) Yun, J.; Lee, H.; Park, Y. S.; Jeong, W.; Jeong, C.-S.; Lee, J.; Lee, J.; Tan, J.; Ma, S.; Jang, G.; et al. Conductive Passivator and Dipole Layer Mixture Enabling High-Performance Stable Perovskite Photoelectrode-Based Solar Water Splitting. *Adv. Energy Mater.* **2023**, *13*, 2301693.
(5) Andrei, V.; Hoye, R. L. Z.; Crespo-Quesada, M.; Bajada, M.; Ahmad, S.; De Volder, M.; Friend, R.; Reisner, E. Scalable Triple Cation Mixed Halide Perovskite-$BiVO_4$ Tandems for Bias-Free Water Splitting. *Adv. Energy Mater.* **2018**, *8*, 1801403.
(6) Yang, H.; Liu, Y. W.; Ding, Y. X.; Li, F. S.; Wang, L. Q.; Cai, B.; Zhang, F. G.; Liu, T. Q.; Boschloo, G.; Johansson, E. M. J.; et al. Monolithic $FAPbBr_3$ photoanode for photoelectrochemical water oxidation with low onset-potential and enhanced stability. *Nat. Commun.* **2023**, *14*, 5486.
(7) Mubarok, M. A.; Choi, Y.; Mehrotra, R.; Kim, Y. J.; Boddu, R. K.; Lee, I.; Kim, J.; Kwak, S. K.; Jang, J. W.; Ryu, J.; et al. Efficient and Stable Tin-Lead Perovskite Photoconversion Devices Using Dual-Functional Cathode Interlayer. *Adv. Energy Mater.* **2024**, *14*, 2302555.
(8) Kim, J. H.; Seo, S.; Lee, J. H.; Choi, H.; Kim, S.; Piao, G.; Kim, Y. R.; Park, B.; Lee, J.; Jung, Y.; et al. Efficient and Stable Perovskite-Based Photocathode for Photoelectrochemical Hydrogen Production. *Adv. Funct. Mater.* **2021**, *31*, 2008277.
(9) Yun, J.; Park, Y. S.; Lee, H.; Jeong, W.; Jeong, C.-S.; Lee, C. U.; Lee, J.; Moon, S.; Kwon, E.; Lee, S.; et al. Efficient and Ultrastable Iodide Oxidation Reaction Over Defect-Passivated Perovskite Photoanode for Unassisted Solar Fuel Production. *Adv. Energy Mater.* **2024**, *14*, 202401055.
(10) Choi, H.; Kim, Y. Y.; Seo, S.; Jung, Y.; Yoo, S. M.; Moon, C. S.; Jeon, N. J.; Lee, S.; Lee, K.; Toma, F. M.; et al. Suppression of Undesired Losses in Organometal Halide Perovskite-Based Photoanodes for Efficient Photoelectrochemical Water Splitting. *Adv. Energy Mater.* **2023**, *13*, 202300951.
(11) Shi, J. J.; Li, Y. M.; Li, Y. S.; Li, D. M.; Luo, Y. H.; Wu, H. J.; Meng, Q. B. From Ultrafast to Ultraslow: Charge-Carrier Dynamics of Perovskite Solar Cells. *Joule* **2018**, *2*, 879−901.
(12) Choi, J.; Jung, W.; Gonzalez-Carrero, S.; Durrant, J. R.; Cha, H.; Park, T. Understanding charge carrier dynamics in organic photocatalysts for hydrogen evolution. *Energy Environ. Sci.* **2024**, *17*, 7999−8018.
(13) Tan, J.; Yang, W.; Oh, Y.; Lee, H.; Park, J.; Boppella, R.; Kim, J.; Moon, J. Fullerene as a Photoelectron Transfer Promoter Enabling Stable TiO_2-Protected Sb_2Se_3 Photocathodes for Photo-Electrochemical Water Splitting. *Adv. Energy Mater.* **2019**, *9*, 201900179.
(14) Liu, T. Y.; Li, W.; Wang, D. Z.; Luo, T. T.; Fei, M. C.; Shin, D.; Waegele, M. M.; Wang, D. W. Low Catalyst Loading Enhances Charge Accumulation for Photoelectrochemical Water Splitting. *Angew. Chem., Int. Ed.* **2023**, *62*, No. e202307909.
(15) Lee, C. U.; Lee, H.; Jeong, C. S.; Ma, S.; Jang, G.; Park, Y. S.; Yun, J.; Lee, J.; Son, J.; Jeong, W.; et al. Enhanced Stability of Spin-Dependent Chiral 2D Perovskite Embedded PV-Biased Anode via Cross-Linking Strategy. *ACS Energy Lett.* **2024**, *9*, 4032−4043.
(16) Min, H.; Lee, D.; Kim, J.; Kim, G.; Lee, K. S.; Kim, J.; Paik, M. J.; Kim, Y. K.; Kim, K. S.; Kim, M. G.; et al. Perovskite solar cells with atomically coherent interlayers on SnO_2 electrodes. *Nature* **2021**, *598*, 444−450.
(17) Di Girolamo, D.; Phung, N.; Kosasih, F. U.; Di Giacomo, F.; Matteocci, F.; Smith, J. A.; Flatken, M. A.; Köbler, H.; Cruz, S. H. T.; Mattoni, A.; et al. Ion Migration-Induced Amorphization and Phase Segregation as a Degradation Mechanism in Planar Perovskite Solar Cells. *Adv. Energy Mater.* **2020**, *10*, 202000310.
(18) Knight, A. J.; Borchert, J.; Oliver, R. D. J.; Patel, J. B.; Radaelli, P. G.; Snaith, H. J.; Johnston, M. B.; Herz, L. M. Halide Segregation in Mixed-Halide Perovskites: Influence of A-Site Cations. *ACS Energy Lett.* **2021**, *6*, 799−808.
(19) Wang, Z. B.; Bae, S.; Baljozovic, M.; Adams, P.; Yong, D.; Service, E.; Moehl, T.; Niu, W. Z.; Tilley, S. D. One-Step Hydrothermal Synthesis of Sn-Doped Sb_2Se_3 for Solar Hydrogen Production. *ACS Catal.* **2024**, *14*, 9877−9886.
(20) Son, M. K.; Steier, L.; Schreier, M.; Mayer, M. T.; Luo, J. S.; Grätzel, M. A copper nickel mixed oxide hole selective layer for Au-free transparent cuprous oxide photocathodes. *Energy Environ. Sci.* **2017**, *10*, 912−918.
(21) Lee, H.; Yang, W.; Tan, J.; Oh, Y.; Park, J.; Moon, J. Cu-Doped NiO_x as an Effective Hole-Selective Layer for a High-Performance Sb_2Se_3 Photocathode for Photoelectrochemical Water Splitting. *ACS Energy Lett.* **2019**, *4*, 995−1003.
(22) Li, H.; Zhou, J. J.; Tan, L. G.; Li, M. H.; Jiang, C. F.; Wang, S. Y.; Zhao, X.; Liu, Y.; Zhang, Y.; Ye, Y. R.; et al. Sequential vacuum-evaporated perovskite solar cells with more than 24% efficiency. *Sci. Adv.* **2022**, *8*, No. eabo7422.
(23) Zhang, F.; Ye, S.; Zhang, H. H.; Zhou, F. F.; Hao, Y. Y.; Cai, H. Z.; Song, J.; Qu, J. L. Comprehensive passivation strategy for achieving inverted perovskite solar cells with efficiency exceeding 23% by trap passivation and ion constraint. *Nano Energy* **2021**, *89*, 106370.
(24) Eames, C.; Frost, J. M.; Barnes, P. R. F.; O'Regan, B. C.; Walsh, A.; Islam, M. S. Ionic transport in hybrid lead iodide perovskite solar cells. *Nat. Commun.* **2015**, *6*, 8497.
(25) Zhao, Y. P.; Yavuz, I.; Wang, M. H.; Weber, M.; Xu, M. J.; Lee, J. H.; Tan, S.; Huang, T. Y.; Meng, D.; Wang, R.; et al. Suppressing ion migration in metal halide perovskite via interstitial doping with a

trace amount of multivalent cations. *Nat. Mater.* **2022**, *21*, 1396−1402.
(26) Lin, Y. Z.; Chen, B.; Fang, Y. J.; Zhao, J. J.; Bao, C. X.; Yu, Z. H.; Deng, Y. H.; Rudd, P. N.; Yan, Y. F.; Yuan, Y. B.; et al. Excess charge-carrier induced instability of hybrid perovskites. *Nat. Commun.* **2018**, *9*, 4981.
(27) Berhe, T. A.; Su, W. N.; Chen, C. H.; Pan, C. J.; Cheng, J. H.; Chen, H. M.; Tsai, M. C.; Chen, L. Y.; Dubale, A. A.; Hwang, B. J. Organometal halide perovskite solar cells: degradation and stability. *Energy Environ. Sci.* **2016**, *9*, 323−356.
(28) Zhidkov, I. S.; Boukhvalov, D. W.; Akbulatov, A. F.; Frolova, L. A.; Finkelstein, L. D.; Kukharenko, A. I.; Cholakh, S. O.; Chueh, C. C.; Troshin, P. A.; Kurmaev, E. Z. XPS spectra as a tool for studying photochemical and thermal degradation in $APbX_3$ hybrid halide perovskites. *Nano Energy* **2021**, *79*, 105421.
(29) Hieulle, J.; Krishna, A.; Boziki, A.; Audinot, J. N.; Farooq, M. U.; Machado, J. F.; Mladenovic, M.; Phirke, H.; Singh, A.; Wirtz, T.; et al. Understanding and decoupling the role of wavelength and defects in light-induced degradation of metal-halide perovskites. *Energy Environ. Sci.* **2024**, *17*, 284−295.
(30) Qin, T. X.; You, E. M.; Zhang, M. X.; Zheng, P.; Huang, X. F.; Ding, S. Y.; Mao, B. W.; Tian, Z. Q. Quantification of electron accumulation at grain boundaries in perovskite polycrystalline films by correlative infrared-spectroscopic nanoimaging and Kelvin probe force microscopy. *Light-Sci. Appl.* **2021**, *10*, 84.
(31) Wang, S. S.; Zhang, S. C.; Shi, X. H.; Yao, C. L.; Jin, D. E.; Gu, D. Y.; Chen, Y. J.; Xu, J. Z.; Xue, J. J.; Wang, R. Self-cleaning Spiro-OMeTAD via multimetal doping for perovskite photovoltaics. *Nat. Commun.* **2025**, *16*, 4167.
(32) Zhang, X. J.; Chen, J. M.; Zheng, L. S.; Liu, Y.; Wang, X. C. Revealing the mechanism between ion migration and the oxidation of hole-transporting layers in high-efficiency perovskite solar cells. *Mater. Sci. Semicon. Proc.* **2023**, *157*, 107310.
(33) Tumen-Ulzii, G.; Qin, C. J.; Matsushima, T.; Leyden, M. R.; Balijipalli, U.; Klotz, D.; Adachi, C. Understanding the Degradation of Spiro-OMeTAD-Based Perovskite Solar Cells at High Temperature. *Sol. RRL.* **2020**, *4*, 2000305.
(34) Ma, F.; Zhao, Y.; Qu, Z. H.; Yu, S. Q.; Chu, Z. M.; Xiong, Z.; Zhou, J. S.; Wei, Z. M.; Zhang, X. W.; You, J. B. Efficient Perovskite Solar Cells with Iodine-Doped Spiro-OMeTAD Hole Transport Layer via Fast Oxidation. *Sol. RRL.* **2023**, *7*, 202300042.
(35) Chen, H. F.; Yan, H. J.; Cai, Y. Q. Effects of Defect on Work Function and Energy Alignment of PbI: Implications for Solar Cell Applications. *Chem. Mater.* **2022**, *34*, 1020−1029.
(36) Jung, M. C.; Raga, S. R.; Ono, L. K.; Qi, Y. B. Substantial improvement of perovskite solar cells stability by pinhole-free hole transport layer with doping engineering. *Sci. Rep-Uk* **2015**, *5*, 9863.

https://doi.org/10.1021/acsenergylett.5c02009
ACS Energy Lett. 2025, 10, 4758−4768